29 May 2010, 8:00 am - 9:30 am

Numerical Analysis of Trampoline Effect in Extreme Ground Motion

Tetsuo Tobita
Kyoto University, Japan

Susumu Iai
Kyoto University, Japan

Tomotaka Iwata
Kyoto University, Japan


Fifth International Conference on
Recent Advances in Geotechnical Earthquake Engineering and Soil Dynamics
and Symposium in Honor of Professor I.M. Idriss
May 24-29, 2010 • San Diego, California

NUMERICAL ANALYSIS OF TRAMPOLINE EFFECT IN EXTREME GROUND MOTION

Tetsuo Tobita
Disaster Prevention Research Institute
Kyoto University
Gokasho, Uji, Kyoto 611-0111, Japan

Susumu Iai
Disaster Prevention Research Institute
Kyoto University
Gokasho, Uji, Kyoto 611-0111, Japan

Tomotaka Iwata
Disaster Prevention Research Institute
Kyoto University
Gokasho, Uji, Kyoto 611-0111, Japan

ABSTRACT

Very large vertical surface acceleration of nearly four times gravity was measured at a strong motion observation station in Iwate Prefecture during the 2008 Iwate-Miyagi Inland, Japan, earthquake (M_w 6.9). The station is located about 3 km southwest of the epicenter and equipped with three-component accelerometers, installed at both the free surface and the bottom of a 260-m borehole. The wave form of the vertical acceleration shows a clearly asymmetric form with large amplitude in the upward direction. Aoi et al. (2008) reported and qualitatively explained the mechanism of this phenomenon by the analogy of bouncing a piece of matter on a trampoline, and thus they called it the "trampoline effect." To simulate this recently discovered nonlinear behavior of the surface ground motion, numerical analysis with a finite-element method has been employed with parameters derived from the borehole data at the station. The analysis successfully simulates the asymmetric vertical motion. Results indicate that the asymmetric motion may be characterized by the existence of a lower bound of negative acceleration, which in most cases corresponds to the acceleration of gravity, and high positive pulses caused by the compression stress of the disturbed surface ground material.

INTRODUCTION

Nonlinear dynamic response is one of the distinguishing characteristics of the ground under strong shaking. The nonlinearity has been reported and investigated by many researchers for more than 40 years. The investigation has been mainly concerned with the following two subjects:

1. The shift of the predominant frequency toward lower frequencies and the decrease of peak amplitudes of acceleration (e.g., Idriss and Seed, 1968; Idriss, 1990).
2. High spikes on horizontal acceleration time histories due to cyclic mobility in relatively dense sand deposit [e.g., 1987 Superstition Hills earthquake (Holzer et al., 1989); 1993 Kushiroki, Japan, earthquake (Iai et al., 1995); 1994 Northridge earthquake (Bardet and Davis, 1996); 1995 Hyogoken Nanbu, Japan, earthquake (Iwasaki and Tai, 1996); 2001 Nisqually earthquake (Frankel et al., 2002); 2004 Niigataken Chuetsu, Japan, earthquake; 2007 Niigataken Chutsu-oki, Japan, earthquake].

The phase-shift of the predominant frequency and the decrease of peak amplitudes (1) are caused by inelastic response of the ground material against large ground strains. This nonlinearity can be indirectly observed by comparing the frequency transfer functions between small and large earthquakes as a shift of the peak frequency of large earthquakes toward lower frequencies. In recent studies, time histories obtained from seismometers forming the vertical array have been intensively employed to derive such transfer functions. Although effects of down-going waves have to be properly considered to derive the transfer functions, simultaneous recordings of the base at a certain depth and surface motions have great advantage for studying local site effects (Bonilla et al., 2005). The mechanism of the nonlinearity has been investigated through laboratory experiments for soils under cyclic loadings, and it has been determined that large, cyclic, shear-strain amplitude causes degradation of soil stiffness. Because of this type of stiffness degradation, the predominant frequency of the ground is shifted down and peak amplitudes are attenuated.

Spiky response on horizontal acceleration records (2) are typically found at a site where the ground material is composed of dense, saturated sand. The results of stress–controlled, undrained, cyclic, triaxial tests for dense sands show an increase of volumetric strain due to stress dilatancy at large strains. This increase of volumetric strain causes rapid

reduction of the excess pore water pressure and results in the rapid recovery of shear strength. When this phenomenon occurs in the real world, the rapid increase of shear stress may be observed as a spiky response on acceleration records (Ishihara 1993). When the spikes appear, other frequency components are attenuated due to build-up of excess pore water pressure reaching to the liquefaction state. These spikes may give over-estimation of the maximum acceleration amplitude and duration of shaking (Bonilla et al. 2005).

In addition to the above-mentioned two types of nonlinear response of the ground, the third nonlinearity under strong ground motion has been recently discovered as being,

3. Asymmetric from the surface vertical acceleration amplitude (Aoi et al., 2008).

In the 2008 Iwate-Miyagi Inland, Japan, earthquake, a very large acceleration amplitude that exceeded 40 m/s^2 (three components combined) was recorded at the KiK-net, IWTH25 station (Figs. 1 and 2). The site is located about 3 km southwest of the epicenter on the hanging wall of the seismic fault. The earthquake was caused by the inland reverse fault with a 30 km strike and 20 km depth. At the IWTH25 station, three-component seismometers are installed at the surface and G.L. -260 m, forming a vertical array. The site is located in a volcanic region, and locally it is on the river sediments underlain by igneous rocks, such as tuff. The recorded wave form of the surface vertical acceleration has large amplitude only in the positive direction. The maximum amplitude of vertical acceleration is four times larger than the acceleration of gravity and two times larger than its horizontal components. Aoi et al. (2008) reported and qualitatively explained the mechanism of this phenomenon by the analogy of bouncing a piece of matter on a trampoline, and they called it the "trampoline effect."

The asymmetric form may be attributed to physical characteristics of granular media, which show asymmetric response against normal compression and tension force. That is, granular media, such as dry sands, have less resistance against tension force. The objective of the present study is to simulate this asymmetric response of the surface vertical acceleration and give physical background to explain this phenomenon.

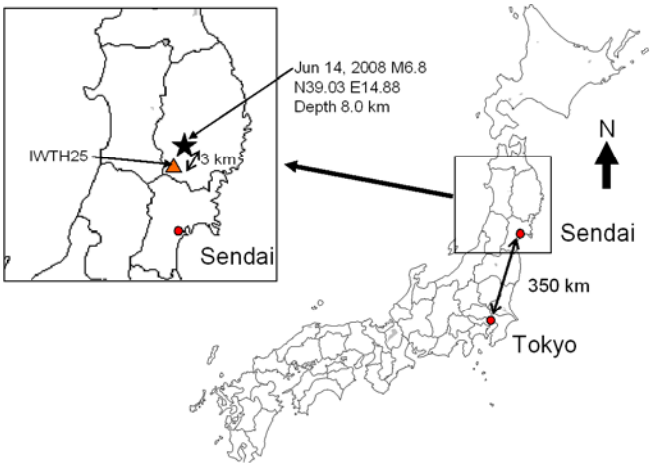

Figure 1. Location of the epicenter of the 2008 Iwate-Miyagi Inland, Japan, earthquake and IWTH25, KiK-net station.

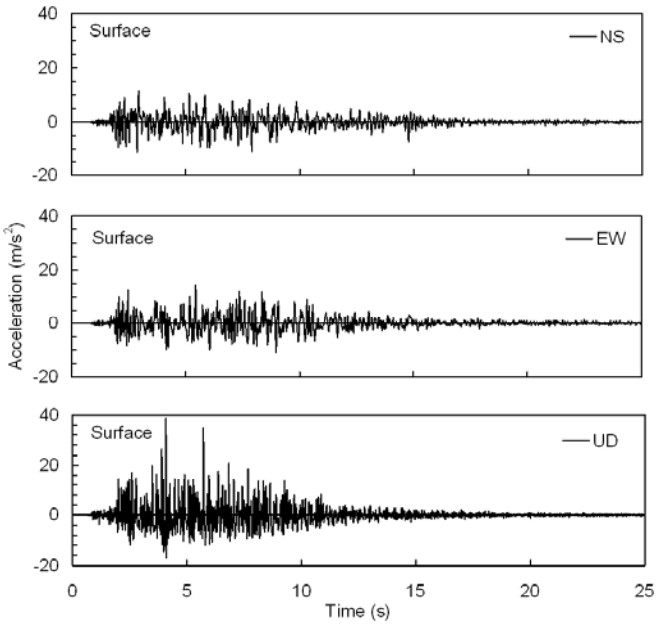

Figure 2. Measured time histories and Fourier amplitudes of surface acceleration at IWTH25 after the 2008 Iwate-Miyagi Inland, Japan, earthquake. Asymmetric amplitude appears on the UD record.

ANALYTICAL MODEL

Numerous analytical models that simulate the nonlinear dynamic ground motion have been proposed over the past 40 years. The equivalent-linear method [SHAKE (Schnabel et al,. 1972), EERA (Bardet et al., 2000)] has been widely used for its simple configuration and precise results for low-to-intermediate levels of ground shaking. To directly simulate the nonlinear stress-strain response of soils, the H-D model (Hardin and Drnevich, 1972) and the R-O model (Ramberg and Osgood, 1943) have been widely used. By combining these nonlinear constitutive models with Masing's law (Masing, 1926), the hysteresis response of soils can be simulated [e.g., NERA (Bardet and Tobita, 2001)]. Iwan (1967), and Mroz (1967) proposed a model for soil nonlinearity and hysteretic behavior by using multiple springs and sliders.

By taking advantage of plasticity theory that started in the field of metal engineering, constitutive models based on the theory of plasticity have been formulated and widely used in the framework of finite-element analysis (Dafalias and Popov, 1975; Hashiguchi, 1980; Matsuoka, 1974; Mroz et al., 1978; Nakai, 1986; Roscoe et al., 1963; Roscoe and Burland, 1968; Sekiguchi and Ohta, 1977; Towhata and Ishihara 1985). These models generally require many parameters, which are more or

less derived from experimental results, to simulate more realistic and complicated behavior of soils.

To simulate soil liquefaction, dynamic solid and fluid coupling behavior has to be incorporated into constitutive modeling. Constitutive models based on the effective stress concept have been proposed for such a material (Iai et al., 1992; Martin et al., 1975; Oka et al., 1999; Prevost, 1985). In these models, by applying dependency on the effective mean stress to the shear behavior of soils, liquefaction as well as dilatant behavior can be successfully simulated.

In this study, the multiple, simple shear mechanism proposed by Towhata and Ishihara (1985) and Iai, et al. (1992) is implemented.

Multiple Simple Shear Mechanism.

The finite-element code called FLIP (Iai et al., 1992) is implemented for nonlinear site response analysis. Total stress analysis is conducted—i.e., there is no excess pore water pressure buildup during shaking. The code utilizes the multiple, simple shear mechanism as the nonlinear constitutive relation (Towhata and Ishihara, 1985). In this model, contact forces between sand particles are idealized by evenly distributed multiple springs (Fig. 3), whose property is characterized by the hyperbolic type. The model automatically accommodates the principal stress rotation, which plays an important roll in the cyclic behavior of anisotropically consolidated sands.

In what follows, the core of the modeling is briefly introduced. Details are found in Ozutsumi (2003). Let us consider the following vectors of stresses and strains:

$$\{\sigma'\}^T = \{\sigma_x' \ \sigma_y' \ \tau_{xy}'\} \quad (1)$$

$$\{\varepsilon\}^T = \{\varepsilon_x \ \varepsilon_y \ \gamma_{xy}\}, \quad (2)$$

where σ_x' and σ_y' are normal stresses, ε_x and ε_y are normal strain, and τ'_{xy} and γ_{xy} are shear stress and shear strain, respectively. The incremental form of the constitutive relationship can be written as follows:

$$\{d\sigma'\} = R_{L/U}\{n_{L/U}\}\{n\}^T\{d\varepsilon\} \quad (3)$$

where the vector $\{n_{L/U}\}$ specifies direction of stress increment, the scalar $R_{L/U}$ defines magnitude of stress increment per unit strain increment along the direction $\{n\}$, and vector $\{n\}$ gives the direction of strains. The subscripts L/U indicate that the components are different in the directions of loading "L" and unloading "U." Iai et al. (1992) postulated that the incremental constitutive relation, Eq. (3), is given by $I + 1$ separate mechanisms for $i = 0$ to I in associated form—i.e., $\{n_{L/U}\} = \{n\}$, as

$$\{d\sigma'\} = \sum_{i=0}^{I} R_{L/U}^{(i)}\{n^{(i)}\}\{n^{(i)}\}^T\{d\varepsilon\}. \quad (4)$$

To specify the volumetric behavior, the first term of Eq. (4), $i = 0$, is independently defined so that Eq. (4) becomes

$$\{d\sigma'\} = K\{n^{(0)}\}\{n^{(0)}\}^T\{d\varepsilon - d\varepsilon_p\} + \sum_{i=1}^{I} R_{L/U}^{(i)}\{n^{(i)}\}\{n^{(i)}\}^T\{d\varepsilon\}, \quad (5)$$

where K is rebound modulus and $\{d\varepsilon_p\}$ is an additional volumetric strain increment due to dilatancy given by

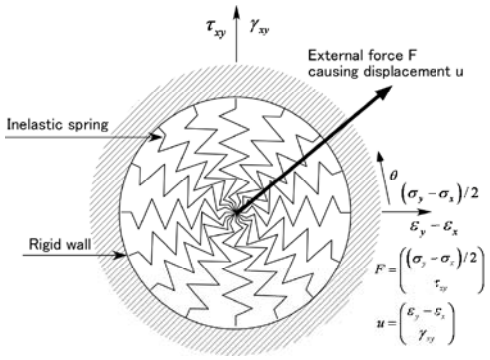

Figure 3. Schematic view of the multiple simple shear mechanism.

$$\{d\varepsilon_p\} = \{d\varepsilon_p/2 \quad d\varepsilon_p/2 \quad 0\}. \quad (6)$$

Direction vectors are given as

$$\{n^{(0)}\}^T = \{1 \quad 1 \quad 0\} \quad (7)$$

$$\{n^{(i)}\}^T = \{\cos\theta_i \quad -\cos\theta_i \quad \sin\theta_i\} \quad \text{(for } i = 1 \text{ to } I\text{)}, \quad (8)$$

where θ_i is the angle of the ith spring from the horizontal axis, which is given as $\theta_i = (i-1)\Delta\theta$ (for $i = 1$ to I), in which $\Delta\theta = \pi / I$. Rewriting Eq. (5) yields,

$$\begin{aligned}\{d\sigma'\} &= \left[K\{n^{(0)}\}\{n^{(0)}\}^T + \sum_{i=1}^{I} R_{L/U}^{(i)}\{n^{(i)}\}\{n^{(i)}\}^T\right]\{d\varepsilon\} \\ &\quad - K\{n^{(0)}\}\{n^{(0)}\}^T\{d\varepsilon_p\} \\ &= [\mathrm{D}]\{d\varepsilon\} - K\{n^{(0)}\}\{n^{(0)}\}^T\{d\varepsilon_p\}\end{aligned} \quad ,(9)$$

in which matrix [D] is

$$[D] = K\{n^{(0)}\}\{n^{(0)}\}^T + \sum_{i=1}^{I} R_{L/U}^{(i)}\{n^{(i)}\}\{n^{(i)}\}^T \quad \text{(for } i = 1 \text{ to } I\text{)}. \quad (10)$$

Rebound modulus K is expressed as

$$K = K_0 \left(\frac{\sigma'}{\sigma_0'} \right)^m , \qquad (11)$$

where K_0 is the rebound modulus at a reference, confining effective stress σ_0', σ' is a current effective stress, and m is a parameter that correlates K and stress ratio σ'/σ_0'. In the framework of the modeling, tangent shear modulus is given as,

$$R_{L/U}^{(i)} = \frac{dF(\gamma_i)}{d\gamma} d\gamma_i \Delta\theta_i , \qquad (12)$$

in which the function $F(\gamma_i)$ is a hyperbolic function that is equivalent to the spring force due to the displacement of a multi-spring in one radian. By assuming Masing's law for cyclic response and defining damping of spring, the shape of function $F(\gamma_i)$ is determined [see Ozutsumi (2003) for details].

In each shear mechanism, loading and unloading conditions can be defined by the sign of

$$d\gamma_i = \left\{ n^{(i)} \right\}^T \{ d\varepsilon \} = \left(d\varepsilon_x - d\varepsilon_y \right) \cos\theta_i + d\gamma_{xy} \sin\theta_i , \qquad (13)$$

where $\gamma_i = \left\{ n^{(i)} \right\}^T \{ \varepsilon \} = \left(\varepsilon_x - \varepsilon_y \right) \cos\theta_i + \gamma_{xy} \sin\theta_i$ is the virtual shear strain of the mechanism $i = 1$ to I. Each tangent modulus depends upon the current state and history of each virtual, simple shear strain γ_i.

In matrix form, Eq. (10) can be written as

$$[D] = K \begin{pmatrix} 1 & 1 & 0 \\ 1 & 1 & 0 \\ 0 & 0 & 0 \end{pmatrix} + G_1 \begin{pmatrix} 1 & -1 & 0 \\ -1 & 1 & 0 \\ 0 & 0 & 0 \end{pmatrix} + G_2 \begin{pmatrix} 0 & 0 & 1 \\ 0 & 0 & -1 \\ 1 & -1 & 0 \end{pmatrix} + G_3 \begin{pmatrix} 0 & 0 & 0 \\ 0 & 0 & 0 \\ 0 & 0 & 1 \end{pmatrix} , \qquad (14)$$

where

$$G_1 = \sum_{i=1}^{I} \frac{dF(\gamma_i)}{d\gamma} \cos^2\theta_i \Delta\theta \qquad (15)$$

$$G_2 = \sum_{i=1}^{I} \frac{dF(\gamma_i)}{d\gamma} \cos\theta_i \sin\theta_i \Delta\theta \qquad (16)$$

$$G_3 = \sum_{i=1}^{I} \frac{dF(\gamma_i)}{d\gamma} \sin^2\theta \Delta\theta . \qquad (17)$$

In the finite-element code, FLIP, if the volumetric strain is positive, judged by the following relation,

$$(\varepsilon_x + \varepsilon_y) - \varepsilon_p \geq 0 \quad \text{(Tension)}, \qquad (18)$$

all of the stress components are set to be zero—i.e., $\sigma_x' = \sigma_y' = \tau_{xy}' = 0$. As will be shown in the next section, this is the property that simulates asymmetric behavior of granular media with no cohesion.

Model Behavior Under Normal Compression and Tension Stresses.

Behavior of the multiple, simple shear model is investigated by applying vertical compression and tension forces to a single element (Fig. 4). Model parameters for this particular study are: shear modulus = 3.2×10^5 (kPa), Poisson's ratio = 0.33, density = 1.8 (t/m^3), and friction angle = 35°. Computation was carried out under drained condition. First, the element is isotropically consolidated with stress σ_0 = 49 (kPa) with nodal constraints illustrated in Fig. 4(a). Then, it is stretched and compressed vertically by enforcing cyclic normal force to nodes 1 and 4 [Fig. 4(b)]. Here, the horizontal displacements of nodes 1 and 4 are constrained. The analytical time step of $\Delta t = 10^{-4}$ was employed. Figure 5(a) depicts time histories of mean stress, $\sigma_m = (\sigma_x + \sigma_y)/2$, and volumetric strain, $\varepsilon_v = \varepsilon_x + \varepsilon_y$, on the left and right vertical axes, respectively. For both strains and stresses, tension is taken as positive. As shown in Fig. 5(a), when the mean stress is zero, tensile strain abruptly increases; that is, the element is vertically stretched. The stress-strain curve in Fig. 5(b) gives another view of this property. Namely, the curve starts at the point indicated as "1" in Fig. 5, where mean stress is -49 kPa, then it is gradually stretched, and once the mean stress reaches zero at "2", volumetric strain abruptly increases up to about 0.3%. On the compression side, in the given range of enforced vertical stress, the stress-strain relationship is within an elastic range following the line whose slope is defined by the rebound modulus of K = 605 MPa.

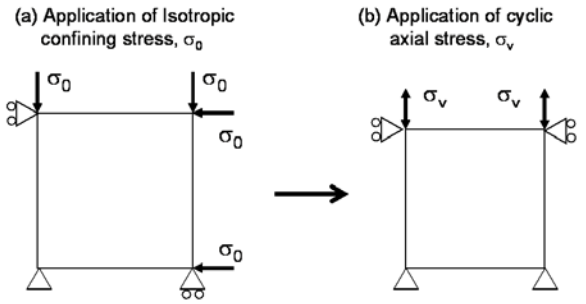

Figure 4. Illustration for application of isotropic confining pressure (a) and cyclic axial stress (b) to a single element.

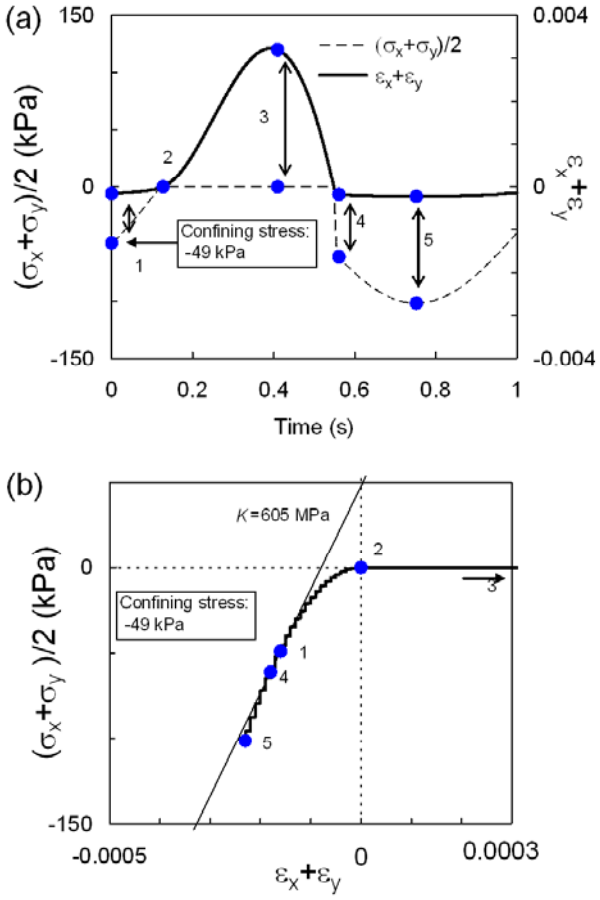

Figure 5. Time histories of (a) mean stress and volumetric strain, and (b) mean stress versus volumetric strain curve.

Model Behavior Against Vertical Input Acceleration.

To simulate the asymmetric vertical ground motion with a simple model, a column 10 m deep with 20 elements is implemented. Each mesh is a square with 0.5 m on a side. The displacement degree of freedom of nodes at the bottom mesh is fixed in both horizontal and vertical directions, and a pair of nodes at the same height was given the same displacement degree of freedom to simulate infinite half-space ground motion. Analysis is carried out by assuming dry conditions. Sinusoidal input acceleration with 10 Hz and the amplitude of 19.6 m/s^2 (= 2 g) is given at the base of the model. In this study, only the vertical motion is given. A computational time step of Δt = 0.001 (s) was employed.

Figure 6(a) is a section of the time histories from 0.5 to 0.8 (s) of volumetric strain ($\varepsilon_v=\varepsilon_x+\varepsilon_y$), input and surface accelerations. In the same manner as Fig. 5(a), Fig. 6(b) shows mean stress [$\sigma_m=(\sigma_x+\sigma_y)/2$] of the surface element, in which the vertical scale of input and surface accelerations (right axis) is magnified 8 times that of Fig. 6(a) for clarity. Here, tension is taken as positive. In Fig. 6(a), tensile strain can be observed while tensile stress is not generated [Fig. 6(b)]. In Fig. 6(b), surface acceleration starts to abruptly increase when the input vertical motion becomes lower than 9.8 m/s^2. This is because at that moment the surface element is free falling and compression force is generated in an element, so reaction to this compression force may create an acceleration pulse in the vertical upward direction. Again, from Fig. 6(b), the lower bound of surface acceleration is limited by the absolute minimum amplitude of vertical input acceleration. Thus, the asymmetric motion of the vertical acceleration can be characterized by the positive pulse in the vertical acceleration due to compression of soils and the existence of a lower bound of negative acceleration.

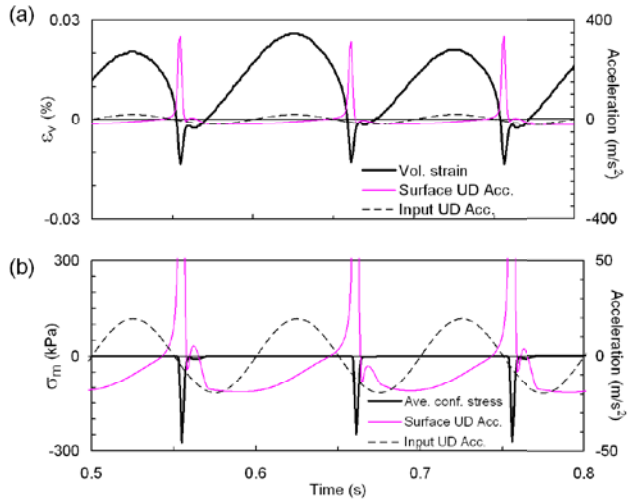

Figure 6. Time histories of (a) volumetric strain, vertical input, and vertical surface acceleration, (b) mean stress, vertical input, and vertical surface acceleration of the surface element. The scale of acceleration in (b) is magnified eight times that of (a).

Figure 7 compares mean stress and volumetric strains of the surface element for various amplitudes of sinusoidal vertical input accelerations. As shown in Fig. 7(a), when the vertical input acceleration is small, response is on the compression side and follows the line whose slope is defined by the initial elastic rebound modulus. As amplitude of input acceleration increases, the curve starts to show nonlinearity. If the amplitude of input vertical acceleration exceeds 9.8 m/s^2, tensile strain appears while mean stress is kept at zero.

Figure 8 shows time histories of the input and surface accelerations for the cases of (a) 19.6 m/s^2 and (b) 9.8 m/s^2 (right axis). In Fig. 8, horizontal solid markers indicate the duration of extension of an element at a certain depth (left axis). When the amplitude of input acceleration is 2 g [Fig. 8(a)], tensile volumetric strains are generated as deep as 10 m, and the duration of tension is much longer than that of compression. In elements, the tensile state appears as soon as the input acceleration turns in the upward direction. Compression starts when the input acceleration decreases from the positive peaks. During compression, on the time histories of surface acceleration, minor peaks are observed that may be simulating the collision between elements. Due to the absolute

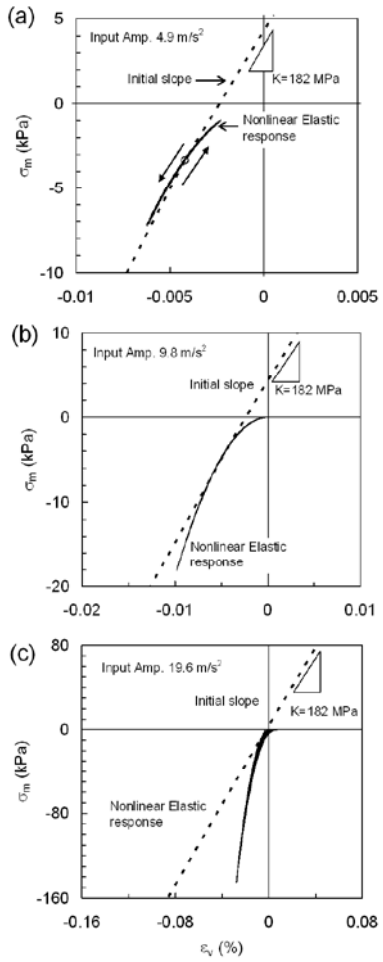

Figure 7. Mean stress versus volumetric strain relationship of the surface element for sinusoidal input acceleration with various amplitudes: (a) 4.9 m/s^2, (b) 9.8 m/s^2 and (c) 19.6 m/s^2.

minimum of input acceleration, surface acceleration also becomes as low as –2 g. If the amplitude of input acceleration is 1 g [Fig. 8(b)], the duration of tension is much shorter, and only the elements whose depth is shallower than G.L. -4 m are in the tensile state, except for the initial cycle in which elements as deep as 10 m are in tensile state.

NUMERICAL ANALYSIS FOR MEASURED EARTHQUAKES

Model parameters for site response analysis of KiK-net, IWTH25 station, such as shear modulus and poisson's ratios, are estimated from the PS velocity profile obtained at the KiK-net, IWTH25 station. Table 1 summarizes model parameters implemented in the following analysis. Based on the velocity profile, the model ground is divided into 8 layers from the surface to G.L. -260 m (Fig. 9). The borehole profile deeper than 120 m shows that the tuff, whose S wave velocity exceeds 1,300 m/s, is predominant. Above it, mud stones and terrace deposit constitute the layers. Densities of material are given as follows: 2.2 t/m^3 for surface cover soil, 2.3 t/m^3 for sediments, and tuff and mud stones are set uniformly at 2.6 t/m^3 (Toyota, 2009).

In the analysis, the ground is modeled with single-column elements (251 elements) whose width is 1 m, and height varies from 0.86 m (layer 1) to 1.09 m (layer 7). With this model ground, the frequency component of the maximum 100 Hz can be properly simulated.

Site Response Analysis for the 2008 Iwate-Miyagi Inland, Japan, Earthquake

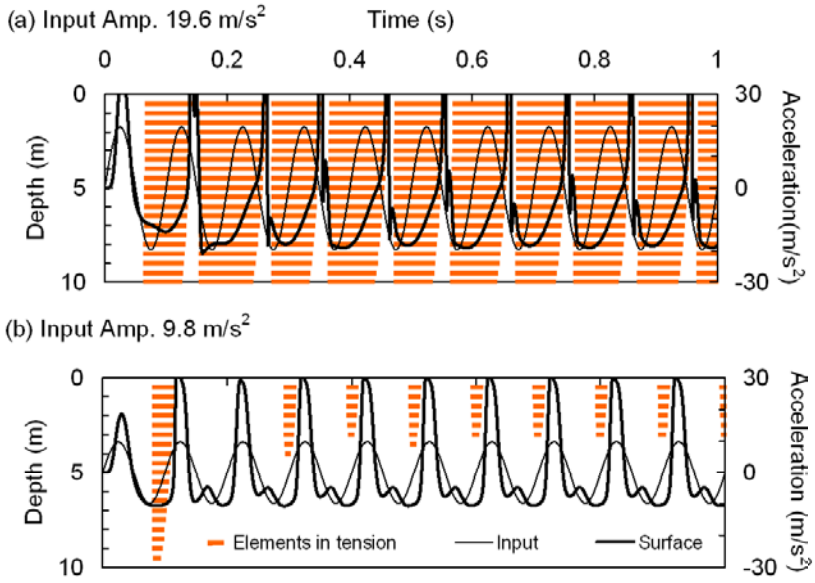

Figure 8. Time histories of input and surface acceleration (right axis) with horizontal bars indicating the duration of tension at the depth of each element (left axis).

Site response analysis is conducted to simulate asymmetric vertical motion observed in the 2008 Iwate-Miyagi Inland, Japan, earthquake. Measured input motion of both horizontal (NS) and vertical (UD) components at the base of the KiK-net array at IWTH25 was input at the base of the model ground with a time step of 0.01 s, which was the same time step as the measured acceleration. As shown in Figs. 10(a) and (b), the computed surface acceleration has an asymmetric shape in the vertical component as compared with the measured one—i.e.,

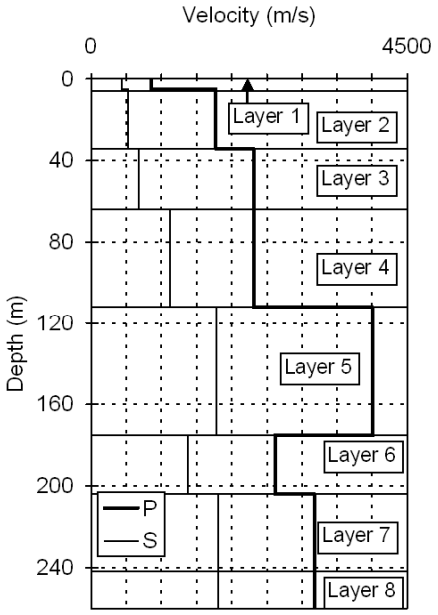

Figure 9. P- and S-wave velocity profile at IWTH25 station and assumed layering system for numerical analysis.

positive spikes and bounded negative amplitude. The maximum amplitude of measured vertical acceleration was about 33 m/s^2, while the one computed over-estimates to be about 61 m/s^2. Negative amplitudes of surface vertical acceleration show, on average, significant agreements between observation and analysis, and it is close to the acceleration due to gravity. This might indicate the temporal free-fall of the ground.

On the measured transfer function of the vertical motion (Fig. 11), in the frequency range of 2 to 10 Hz, the site amplification factor varies in a limited range between 3 and 6, and there is no clear peak, while there is a clear peak at about 4.5 Hz in computation. The computed peak frequency is consistent with the one for small input motion which was separately conducted and not shown in the present paper. Hence, it is thought to be a dominant frequency of the model ground against vertical motion. One of the possible causes of this discrepancy may be the heterogeneity in the real ground. Except for the peak at 4.5 Hz, the computed transfer function over 10 Hz shows good agreement with the measured one. Higher-frequency components are properly simulated because input acceleration might be large enough for higher-frequency components to be transmitted to the surface.

To see the model behavior of the surface element, computed time histories from 4.5 to 5 (s) of volumetric strain and mean stress with computed vertical surface acceleration are plotted in Figs. 12(a) and (b). Also, the mean stress and volumetric strain relationship is depicted in Fig. 12(c). When the surface acceleration is negative (4.62 to 4.72 s), volumetric strain indicated by numbers 3 and 4 in Fig. 12(a) is positive, while the mean stress is kept as zero [Fig. 12(b)]. When the surface element is under compression indicated by numbers 5 to 7 in Fig. 12(b), positive spikes appear on the surface vertical acceleration. In the same manner as the simple example mentioned earlier, the mean stress and volumetric strain relation [Fig. 12(c)] follows a quadratic curve that is a volumetric stress and strain relationship specified by Eq. (11).

Computed time histories of vertical acceleration at the top of each layer are shown in Fig. 13, together with solid markers indicating the duration and depth of elements whose volumetric strain is in tension. From the time histories, asymmetry of the amplitude starts to appear at the depth shallower than G.L. -64 m. From the travel-time curve drawn with the thick dotted line in Fig. 16, it is clearly seen that reflected spiky waves at the surface are transmitted as down-going waves with large amplitudes and that they interfering with incident waves.

Table 1. Model Parameter of the Ground Profile at the KiK-net, IWTH25 Station

Layer No.	Depth of bottom of layer	Wave velocity		Density	Poisson's ratio	Shear modulus	Bulk moduls	Reference confining stress		Friction angle	Rayleigh damping factor: β
		P	S	ρ	ν	G	K	σ_r'	h_{max}		
	(m)	(m/s)	(m/s)	(t/m^3)		(kPa)	(kPa)	(kPa)		(deg.)	
1	6.00	850.0	430.0	2.2	0.33	406780	1047127	9.9			
2	34.0	1770	530.0	2.3	0.45	646070	6344243	58.2			
3	64.0	2310	680.0	2.6	0.45	1183282	12077371	115.8			
4	112	2310	1120	2.6	0.35	3252659	9499628	209.1	0.2	45	0.0015
5	175	4010	1780	2.6	0.38	8107936	30338395	330.0			
6	204	2620	1380	2.6	0.31	4873360	11068187	385.7			
7	242	3180	1810	2.6	0.26	8383540	14699578	458.6			
8	260	3180	1810	2.6	0.26	8383540	14699578	493.2			

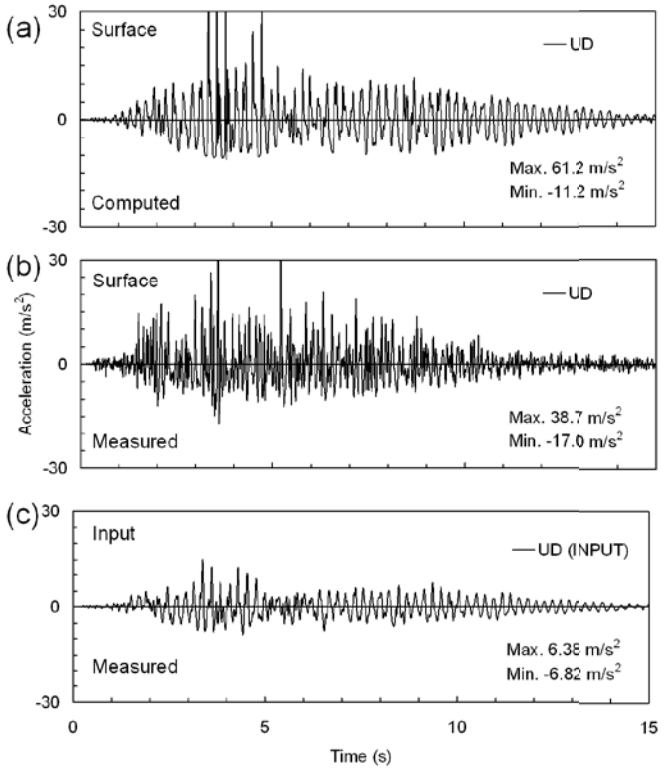

Figure 10. Computed (a) and measured (b) surface acceleration, and measured base acceleration (C) for the 2008 Iwate-Miyagi Inland earthquake.

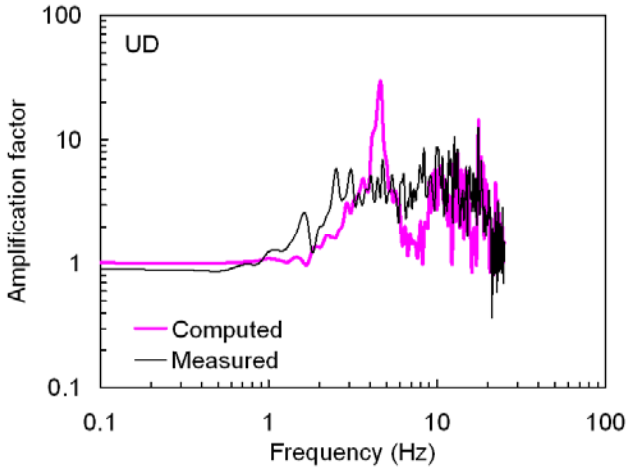

Figure 11. Transfer functions of measured and computed vertical acceleration for the 2008 Iwate-Miyagi Inland earthquake.

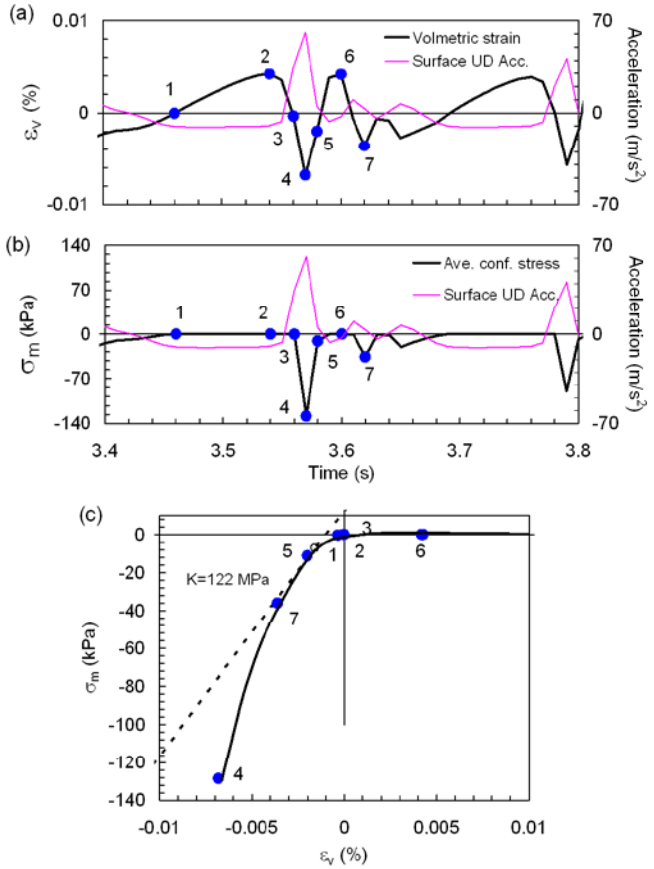

Figure 12. Computed time histories from 4.5 to 5.0 (s); (a) volumetric strain, (b) mean stress. In (a) and (b), computed UD components of surface acceleration are plotted as a reference. (c) Mean stress versus volumetric strain relationship.

CONCLUSIONS

During the 2008 Iwate-Miyagi Inland, Japan, earthquake, a very large acceleration record, which exceeded 40 m/s^2 (three components combined), was observed at the vertical array site, KiK-net, IWTH25 station. The surface vertical acceleration record had asymmetric amplitude. In the present study, analytical research was carried out for this newly discovered nonlinear site response associated with the vertical strong ground motion.

First, model behavior against normal compression and tension was examined by using a single element. Then response against vertical motion was investigated by using a simple column mesh with 10 m depth and a sinusoidal input motion of 10 Hz. When the amplitude of input acceleration was 2 g, tensile volumetric strains were generated as deep as 10 m, and the duration of tension was much longer than compression. On the other hand, if the amplitude of input acceleration was 1 g, the duration of tension was much shorter, and only the elements whose depths were shallower than G.L. -4 m fell in

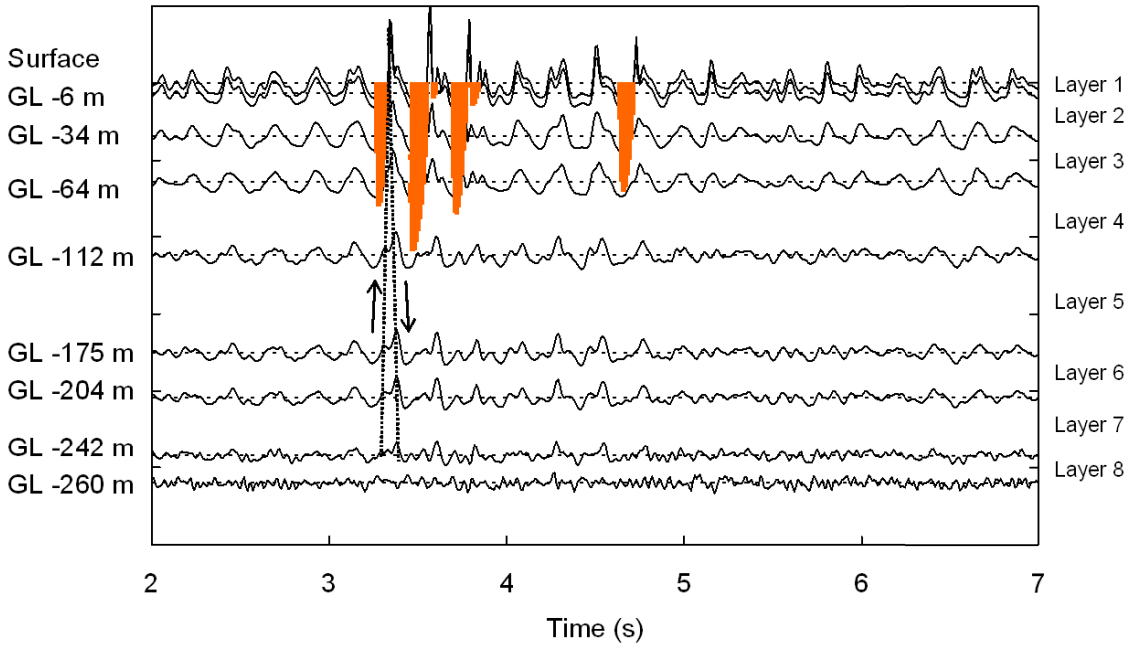

Figure 13. Computed vertical acceleration at the top of each layer, except for the base input acceleration, which is the measured one. Thick vertical sections at time between 3 to 5 seconds indicate the ground elements whose volumetric strain is more than zero.

the tensile state. In the case of the 2-g input motion, due to the absolute minimum of input acceleration, surface acceleration also became as low as –2 g. The analytical results indicated that the asymmetry in vertical surface acceleration might be characterized by the positive pulse due to compression stress applied to the ground material and the existence of a lower bound of negative acceleration, which in most cases corresponds to the acceleration of gravity.

Then, the observed asymmetric ground motion was simulated with a model ground of a column whose model parameters were derived from the borehole profile at the vertical array, KiK-net, IWTH25 site. The ground model was constituted of eight layers from the surface to G.L. -260 m, which was assumed to be the base of the IWTH25 station. With the base records of NS and UD components as input motions, site response analysis was conducted. For horizontal motion, the dominant frequency of the transfer function at about 6 Hz agreed well with the measured one. Vertical acceleration at the surface clearly showed asymmetric form, as can be seen in the observed acceleration. However, on measured transfer function of the vertical motion, in the frequency range of 2 to 10 Hz, the transfer function showed no clear peaks, while in computation a peak at about 4.5 Hz appeared. The computed peak frequency was consistent with the one for small input motion. Hence, it was thought to be a dominant frequency of the model ground against vertical motion. One of the possible causes of this discrepancy might be the heterogeneity in the real ground. Except for the peak at 4.5 Hz, a computed transfer function over 10 Hz showed good agreement with the measured one. From the time histories, asymmetry of the amplitude appeared at depths shallower than G.L. -64 m.

In computation, the asymmetry of the vertical motion was successfully simulated with the assumption included in the constitutive relation; that is, all of the stress components are set to be zero when elements are under tensile volumetric strains. In reality, it may be attributed to physical characteristics of granular media, which show asymmetric response between normal compression and tension force.

REFERENCES

Aoi, S., T. Kunugi, and H. Fujiwara [2008]. “Trampoline effect in extreme ground motion”, *Science* 322, 727–730.

Bardet, J. P., and C.A. Davis [1996], “Performance of San Fernando dams during the 1994 Northridge Earthquake”, *J. Geotech. Eng. Div., ASCE* 122, 554–564.

Bardet, J. P., K. Ichii, and C. H. Lin [2000]. “EERA: A computer program for equivalent-linear earthquake site response analyses of layered soil deposits”, *A report to Department of Civil Engineering, University of Southern California*, http://geoinfo.usc.edu/gees.

Bardet, J. P., and T. Tobita [2001]. ”NERA: A computer program for nonlinear earthquake site response analysis of layered soil deposits”, *Department of Civil Engineering, University of Southern California*, http://geoinfo.usc.edu/gees.

Bonilla, L., Fabian, Archuleta, R., J. and Lavallee, D. [2005]. "Hysteretic and dilatant behavior of cohesionless soils and their effects on nonlinear site response: Field data observations and modeling", *Bull. Seism. Soc. Am.* 95, 2373–2395.

Dafalias, Y. F. and E. Popov [1975]." A model of nonlinearity hardening materials for complex loading", *Acta Mech.* 21, 173–192.

Frankel, A. D., D. L. Carver, and R. A. Williams [2002]. "Nonlinear and linear site response and basin effects in Seattle for the M 6.8 Nisqually, Washington earthquake", *Bull. Seism. Soc. Am.* 92, 2090–2109.

Hardin, B. O., and V. P. Drnevich [1972]. "Shear modulus and damping in soils: Design equations and curves", *J. Soil Mech. Found. Div.* 1, 2–89.

Hashiguchi, K. [1980]. "Constitutive equation of elastoplastic materials with elasto-plastic transition", *J. Appl. Mech., ASME* 102, 266–272.

Holzer, T. L., T. L. Youd, and T. C. Hanks [1989]. "Dynamic liquefaction during the 1987 Superstition Hills, California, earthquake", *Science* 244, 56–59.

Iai, S., Y. Matsunaga, and T. Kameoka [1992]. "Strain space plasticity model for cyclic mobility", *Soils Found.* 32 1–15.

Iai, S., T. Morita, T. Kameoka, Y. Matsunaga, and K. Abiko [1995]. "Response of a dense sand deposit during 1993 Kushiro-oki earthquake", *Soils Found.* 35, 115–131.

Idriss, I. M., and H. B. Seed [1968]. "Analysis of ground motions during the 1957 San Francisco earthquake", *Bull. Seism. Soc. Am.* 58, 2013–2032.

Idriss, I. M. [1990]. "Response of soft soil sites during earthquakes", *Proceedings of the H. Bolton Seed Memorial Symposium* 2, J. M. Duncan (Editor), BiTech Publisher, Vancouver, 273–289.

Ishihara, K. [1993]. "Liquefaction and flow failure during earthquakes", The 33rd Rankine Lecture, *Geotechnique* 43, 351–415.

Iwan, W. D. [1967]. "On a class of models for the yielding behavior of continuous and composite systems", *J. Appl. Mech. ASME* 34, 612–617.

Iwasaki, Y., and M. Tai [1996]. "Strong motion records at Kobe Port Island", *Special Issue of Soils and Foundations, Japanese Geotechnical Society*, 29–40.

Martin, G. R., W. D. L. Finn, and H. B. Seed [1975]. "Fundamentals of liquefaction under cyclic loading", *J. Geotech. Eng. Div., ASCE* 101, 423–438.

Masing, G. [1926]. "Eiganspannungen und verfestigung beim messing", *Proceedings of Second International Conference of Applied Mechanics*, 322–335.

Matsuoka, H. [1974]. "Stress-strain relationship of sands based on the mobilized plane", *Soils Found* 14, 47–61.

Mroz, Z. [1967]. "On the description of anisotropic workhardening", *J. Mechanics and Physics of solids* 15, 163–175.

Mroz, Z., V. A. Norris and O. C. Zienkiewicz [1978]. "An anisotropic hardening model for soils and its application to cyclic loading", *Int. J. Numer. Anal. Meth. Geomech.* 2, 203–221.

Nakai, T. [1986]. "A generalized elastoplastic constitutive model for clay in a three-dimensional stresses", *Soils Found.* 26, 81–89.

Oka, F., A. Yashima, Y. Tateishi, Y. Taguchi, and S. Yamashita [1999]. "A cyclic elasto-plastic constitutive model for sand considering a plastic-strain dependence of the shear modulus", *Geotechnique* 49, 661–680.

Ozutsumi, O. [2003]. "Development of an numerical method for earthquake damage estimation of soil and structure systems on liquefiable ground", *Doctor's dissertation submitted to the Department of Civil and Earth Resources Engineering, Kyoto University* (in Japanese).

Prevost, J. H. [1985]. "A simple plasticity theory for frictional cohesionless soils", *Soil Dynam. Earthquake Eng.* 4, 9–17.

Ramberg, W. and Osgood, W. R. [1943]. "Description of stress-strain curve by three parameters", *Tech. Note 902, National Advisory committee for Aeronautics, Washington, D.C.*

Roscoe, K. H., Schofield, A. N. and Thurairajah, A. [1963]. "Yielding of clay in states wetter than critical", *Geotechnique* 13, 211–240.

Roscoe, K. H., and J. B. Burland [1968]. "On the generalised stress-strain behaviour of "wet" clay", *Engineering Plasticity*, Cambridge Press, 535–609.

Schnabel, P. B., J. Lysmer, and H. B. Seed [1972]. "SHAKE-A computer program for earthquake response analysis of horizontally layered sites", *Earthquake Engineering Research Center, College of Engineering, University of California, Berkeley*, Report No. EERC 72-12.

Sekiguchi, H., and H. Ohta [1977]. "Induced anisotropy and time dependency in clays", *Proc. 9th ICSMFE*, Speciality Session 9, 229–238.

Towhata, I., and K. Ishihara [1985]. “Modelling soil behaviour under principal stress axes rotation”, *Proceedings of 5th International Conference on Numerical Methods in Geomechanics*, Nagoya 1, 523–530.

Toyota, H. [2009]. Nagaoka University of Technology, *Personal communication.*